Molecular Crystals and Liquid Crystals
Publication details, including instructions for authors and subscription information:
http://www.tandfonline.com/loi/gmcl16

Anisotropic Ultrasound Propagation in a Cholesteric Liquid Crystal

S. Bhattacharya [a] , I. Muscutariu [a d] & J. B. Ketterson [b c]

[a] Department of Physics, Northwestern University, Evanston, Illinois, 60201

[b] Department of Physics, Materials Research Center Northwestern University, Evanston, Illinois, 60201

[c] Argonne National Laboratory, Argonne, Illinois, 60439

[d] Physics Department, University of Timisoara, Timisoara, 1900, Romania

Version of record first published: 19 Oct 2010.

To cite this article: S. Bhattacharya , I. Muscutariu & J. B. Ketterson (1978): Anisotropic Ultrasound Propagation in a Cholesteric Liquid Crystal, Molecular Crystals and Liquid Crystals, 44:1-2, 1-22

To link to this article: http://dx.doi.org/10.1080/00268947808084964

Mol. Cryst. Liq. Cryst., 1978, Vol. 44, pp. 1–22

Printed in Holland

Anisotropic Ultrasound Propagation in a Cholesteric Liquid Crystal†

S. BHATTACHARYA and I. MUSCUTARIU‡

Department of Physics, Northwestern University, Evanston, Illinois 60201

and

J. B. KETTERSON

Department of Physics and Materials Research Center Northwestern University, Evanston, Illinois 60201 and Argonne National Laboratory, Argonne, Illinois 60439

(*Received January 2, 1977; in final form May 7, 1977*)

We report here a detailed study of the propagation of longitudinal ultrasound through a magnetically aligned cholesteric liquid crystal (a mixture of cholesteryl chloride and cholesteryl myristate, 1.75:1 by weight). The observed velocity anisotropy is tentatively attributed to dispersion and an attenuation anisotropy was observed for the first time. The temperature dependence of several elastic constants and combinations of viscosity coefficients was determined. A new expression for the attenuation was derived from the hydrodynamic equations, and from a twisted nematic model. A more detailed report of the acoustic Brillouin zone effect is also presented.

INTRODUCTION

In recent years, many hydrodynamic theories have been proposed for liquid crystals. The generalization of hydrodynamics to include liquid crystals was first studied by Erickson and Leslie.[1] Subsequently Lubensky and Martin and co-workers [2–5] modified and generalized the formalism.

† Work supported by the National Science Foundation through Grant No. DMR-74-13186, the Northwestern Materials Research Center, and the U.S. Energy Research and Development Agency.

‡ Visiting Fulbright Scholar. Permanent Address: Physics Department, University of Timisoara, Timisoara 1900, Romania.

Of the different symmetries of liquid crystals, nematics have been the most extensively studied, both theoretically and experimentally. In spite of some differences among the different theories, there is general agreement in the hydrodynamic limit ($\omega, q \to 0$). Ultrasonic waves, by virtue of their low frequency, serve as very effective probes for investigating the low-frequency, long-wavelength-behavior of liquid crystals.

Extensive work has been done on nematics[6-9] and theoretical predictions, such as the absence of a velocity anisotropy in the hydrodynamic limit, have been confirmed experimentally.[14] Some experimental results [10,11] in smectic-A liquid crystals are also available in the literature. Cholesterics, however, have been very sparsely studied.[19] Most experiments were performed on unaligned materials and therefore the anisotropic properties remained obscure.

A new physical effect, not possible in nematics, can be observed in cholesterics. This is the so-called Brillouin zone effect.[12] For materials and temperatures such that the cholesteric pitch length is comparable to the sound wave length, a "Bragg like" interaction can occur which results in anomalies in the acoustic attenuation.

There are several problems in working with cholesterics. Firstly, most cholesterics have positive magnetic anisotropy. The molecules tend to align with their long axes parallel to the applied magnetic field and thus the helix axis aligns perpendicular to the field. This situation may not, in general, produce a completely aligned sample since several domains, or textures, having their helix axes at arbitrary angles in the plane perpendicular to the field could exist. In addition, under such a situation the field distorts the helical structure and above a certain critical field, H_c, a Fredericks transition takes place.[13] For such materials, a uniform macroscopic alignment is not obtainable.

Secondly, cholesterics are extremely viscous and for a finite geometry boundary effects become very prominent. It was observed that by rotating the magnetic field direction in the cholesteric phase complete reorientation was not obtained.[14]

Thirdly, the high viscosity gives rise to very high attenuation, and therefore measurements at higher frequencies become difficult with a sufficiently long acoustic path-length.

In the present paper we report a detailed study of anisotropic ultrasound propagation through a magnetically aligned cholesteric liquid crystal. The material chosen was a mixture of cholesteryl chloride and cholesteryl myristate (hereafter referred to as CC-CM) (1.75:1 by weight) which becomes cholesteric at 68°C upon cooling. This material is known [15] to have negative magnetic anisotropy. The long-axes of the molecules align perpendicular to the field, and the helix axis is then parallel to the field, i.e., macroscopic alignment can be obtained.

Because of the large attenuation at lower temperatures, all measurements were done at 4 MHz.

In the first section we briefly describe the sound propagation problem. In the second section we discuss the hydrodynamic theory we used to analyze our data. A brief description of the so-called "twisted nematic" model is also given. In Section 3 we present our data on the anisotropic longitudinal sound propagation at relatively high temperatures in the cholesteric phase. In Section 4 we give a somewhat more detailed report of the Brillouin zone effect than has been reported previously.[12]

Section I. Sound propagation: A phenomenological approach

A detailed account of this description will be found in Ref. 14; here we mention only the final results. For a system with uniaxial symmetry and for the mode that is a pure longitudinal wave along the symmetry axis and is predominantly longitudinal for off-axis propagation, the velocity and attenuation coefficient are given by

$$2V^2\rho_0 = C_{11}\sin^2\theta + C_{44} + \{[(C_{11} - C_{44})\sin^2\theta - (C_{33} - C_{44})\cos^2\theta]^2 + 4(C_{13} + C_{44})^2\sin^2\theta\cos^2\theta\}^{\frac{1}{2}} \quad (1)$$

$$\alpha = \frac{\omega^2}{2V^3\rho_0}[D_{11}\sin^2\theta + D_{33}\cos^2\theta + (2D_{13} + 4D_{44} - D_{11} - D_{33})\sin^2\theta\cos^2\theta] \quad (2)$$

The angle θ is measured from the 3-axis which is the uniaxial symmetry axis. We also assume that the velocity anisotropy is small and the mode propagates many wavelengths without excessive attenuation, i.e., $C_{ij} \gg \omega D_{kl}$. If the sound velocity and attenuation are measured as a function of θ, then the combinations of C's and D's can be determined by least squares techniques.

Section II. Theory

In order to obtain an expression for sound attenuation in cholesterics we have to consider the periodicity of the helix axis. We assume that locally in the 1-2 plane cholesterics have nematic ordering. However as one moves along the 3-direction the director twists around the pitch axis. If we consider the density and the compressibility to be uniform and not periodic, in the first approximation there would be no effect of the periodic structure.

In the event that the viscosity tensor is periodic one would expect to see the effect of the periodicity in the sound attenuation when the component of sound wave-vector, q_s, along the 3-direction matches the Brillouin zone spacing.

When the wavelength of sound is much larger than the pitch (which is usually the case) the sound-attenuation should be anisotropic, but no effect of periodicity will be seen. In that situation we can imagine the cholesteric to be nothing but a twisted nematic and the attenuation of cholesterics will be the same as a nematic with the varying director orientation averaged out.

Parsons and Hayes[16] obtained approximate expressions for sound attenuation for different ranges of the sound wave vector $\mathbf{q}_s$ as compared to the pitch wave vector, or Brillouin zone spacing, $q_0 = \pi/P$ where P is the pitch. The model they chose to work with is the Leslie incompressible nematic with the addition of a bulk viscosity term in the dissipative part of the stress-tensor. In particular, they neglected any anisotropy in the bulk viscosity; this approximation may not be totally correct. For the nematics paraazoxyanisole and paraazoxyphenetole, Kemp and Letcher[7] showed that the two bulk viscosity coefficients ν_5 and $\nu_4 - \nu_2$ are not identical and are further two orders of magnitude higher than the shear viscosity coefficients. Therefore anisotropy in the bulk viscosity cannot be neglected.

We will now extend the work of Parsons and Hayes on the attenuation of sound in cholesteric liquid crystals to account for bulk viscosity effects. We start with the equation of continuity

$$\frac{\partial \rho}{\partial t} + \nabla \cdot \mathbf{g} = 0 \tag{3}$$

where ρ is the density, $\mathbf{g} \equiv \rho \mathbf{v}$, and $\mathbf{v}$ is the fluid velocity. We will also need the momentum transport equation given by

$$\frac{\partial g_i}{\partial t} + \nabla_j \sigma_{ij} = 0 \tag{4}$$

where $\sigma_{ij} = \sigma_{ij}^R + \sigma_{ij}^D$ and σ_{ij}^R and σ_{ij}^D are respectively the reactive and dissipative parts of the stresstensor σ_{ij}. In the first approximation, the material is uniform and we can ignore director fluctuations. In this limit

$$\sigma_{ij} = p\delta_{ij}. \tag{5}$$

Taking the divergence of Eq. (4) and inserting the time derivative of Eq. (5) we obtain

$$\frac{\partial^2 \rho}{\partial t^2} + \nabla^2 p + \nabla_i \nabla_j \sigma_{ij}^D = 0. \tag{6}$$

We consider small amplitude waves and expand

$$\rho = \rho_0 + \rho'$$

and

$$p = p_0 + p'$$

where the primed quantities represent small deviations from equilibrium. For adiabatic small amplitude sound propagation, we can write $p' \cong V^2\rho'$ where $V^2 \equiv (\partial p/\partial\rho)_s$. Assuming periodic motion of the form $e^{-i\omega t}$, Eq. (6) becomes

$$\omega^2\rho' + V^2\nabla^2\rho' + \nabla_i\nabla_j\sigma_{ij}^D = 0 \tag{7}$$

For σ^D we use the expressions of Forsters, *et al.*,[4]

$$\begin{aligned}\delta\sigma_{ij}^D = &-2\nu_2 A_{ij} - 2(\nu_3 - \nu_2)[A_{ik}n_k n_j + A_{jk}n_i n_k] - (\nu_4 - \nu_2)\delta_{ij}A_{kk} \\ &-2(\nu_1 + \nu_2 - 2\nu_3)n_i n_j n_k n_l A_{kl} - (\nu_5 - \nu_4 + \nu_2)[\delta_{ij}n_k n_l A_{kl} + n_i n_j A_{kk}]\end{aligned} \tag{8}$$

where the n_i's are the components of the director and

$$A_{ij} = \tfrac{1}{2}[\nabla_j v_i + \nabla_i v_j].$$

For a cholesteric liquid crystal whose helix axis is along the z-direction the director $\hat{n}$ has the following components

$$n_x = \cos(q_0 z); \qquad n_y = \sin(q_0 z); \qquad n_z = 0. \tag{9}$$

Substituting Eq. (8) in Eq. (7) using Eq. (9) and $\nabla\cdot\mathbf{v} \cong (i\omega/\rho_0)\rho'$ from Eq. (3) we obtain

$$\begin{aligned}&\left[\omega^2 - V^2\nabla^2 + \frac{\nu_4 + \nu_2}{\rho_0}\, i\omega\nabla^2 - \frac{2(\nu_3 - \nu_2)}{\rho_0}\right. \\ &\times\left\{(1 + \cos 2q_0 z)i\omega\frac{\partial^2}{\partial x^2} + \frac{2iV^2}{\omega}q_0 \sin 2q_0 z\frac{\partial^2}{\partial x^2}\frac{\partial}{\partial z}\right\} - \frac{(\nu_5 - \nu_4 + \nu_2)}{\rho_0} \\ &\times\left\{(1 + \cos 2q_0 z)i\omega\frac{\partial^2}{\partial x^2} + \frac{iV^2}{\omega}q_0^2\cos 2q_0 z\frac{\partial^2}{\partial x^2} + \frac{2iV^2}{\omega}q_0 \sin 2q_0 z\frac{\partial^2}{\partial x^2}\frac{\partial}{\partial z}\right\} \\ &\left.+ \frac{2(\nu_1 + \nu_2 - \nu_3)}{\rho_0}\frac{iV^2}{\omega}\frac{\partial^2}{\partial x^2}\left(\frac{\partial^2}{\partial x^2}\right)\left[\frac{1}{8}(3 + 4\cos 2q_0 z + \cos 4q_0 z)\right]\right] \\ &\times \rho'(r, t) = 0.\end{aligned} \tag{10}$$

We take the Fourier transform of the density fluctuation

$$\rho'(\mathbf{r}, t) = \int b(\mathbf{q})e^{i\mathbf{q}\cdot\mathbf{r} - i\omega t}\, d\mathbf{q}.$$

We restrict $\mathbf{q}$ to lie in the $x - z$ plane with q_1 the component along the x-direction. The translational invariance of the liquid along x implies pure plane wave motion in this direction. Thus

$$\rho'(\mathbf{r}, t) = e^{iq_1 x}\int g(q_3)e^{iq_3 z - i\omega t}\, dq_3.$$

With this substitution then Eq. (10) becomes

$$\int [H_0 + H']g(q_3)e^{iq_3z}\,dq_3 = 0 \tag{11}$$

where

$$H_0 \equiv \omega^2 - V^2q^2 + \frac{\nu_4 + \nu_2}{\rho_0} i\omega q^2 + \frac{2(\nu_3 - \nu_2)}{\rho_0} i\omega q_1^2 + \frac{\nu_5 - \nu_4 - \nu_2}{\rho_0} i\omega q_1^2 + \frac{2(\nu_1 + \nu_2 - 2\nu_3)}{\rho_0} \frac{3}{8} \frac{iV^2}{\omega} q_1^4 \tag{12}$$

and

$$H' \equiv \frac{\nu_5 - \nu_4 - 2\nu_3 - \nu_2}{\rho_0} \left(i\omega q_1^2 \cos 2q_0 z - \frac{2V^2q_1^2}{\omega} q_0 q_3 \sin 2q_0 z \right) + \frac{\nu_1 + \nu_2 - 2\nu_3}{\rho_0} \frac{iV^2q_1^4}{\omega} \cos 2q_0 z + \frac{\nu_5 - \nu_4 + \nu_2}{\rho_0} 2q_0^2 \frac{iV^2}{\omega} q_1^2 \cos 2q_0 z. \tag{13}$$

For the asymptotic case, i.e., $q_3 \gg q_0$ or $q_3 \ll q_0$ we can ignore the periodic terms of H'. Setting $H_0 = 0$ and writing $q_1 = q_s \sin\theta$, $\omega = Vq_s - i\Gamma_q$, and solving for Γ_q, we obtain

$$\Gamma_q = \frac{q_s^2}{2\rho_0} [(\nu_4 + \nu_2) + (\nu_5 - \nu_4 + 2\nu_3 - \nu_2)\sin^2\theta + \tfrac{3}{4}(\nu_1 + \nu_2 - 2\nu_3)\sin^4\theta] \equiv (\Gamma_q)_0. \tag{14}$$

We now study the case where Bragg effects are important. We multiply Eq. (11) by $e^{-iq_3'z}$ and integrate over dz followed by an integration over dq_3 to obtain

$$g(q_3')H_0 + H_+ g(q_3' + 2q_0) + H_- g(q_3' - 2q_0) = 0 \tag{15}$$

where

$$H_+(q_1, q_3' + 2q_0) \equiv i\omega q_1^2 \frac{\alpha}{2} + \frac{iV^2q_1^4}{\omega} \frac{\beta}{2} + \frac{\alpha}{2} \frac{2iV^2q_1^2}{\omega} (q_3' + 2q_0) + \frac{\gamma}{2} \frac{iV^2}{\omega} 2q_0^2 q_1^2 \tag{16}$$

and

$$H_-(q_1, q_3' - 2q_0) \equiv i\omega q_1^2 \frac{\alpha}{2} + \frac{iV^2q_1^4}{\omega} \frac{\beta}{2} - \frac{\alpha}{2} \frac{2iV^2q_1^2}{\omega} (q_3' - 2q_0) + \frac{\gamma}{2} \frac{iV^2}{\omega} 2q^2 q_1^2$$

with

$$\alpha \equiv (\nu_5 - \nu_4 - 2\nu_3 - \nu_2)/\rho_0$$
$$\beta \equiv (\nu_1 + \nu_2 - 2\nu_3)/\rho_0$$

and

$$\gamma \equiv (\nu_5 - \nu_4 + \nu_2)/\rho_0.$$

Setting $q_3' = \pm q_0$ in the above and retaining only the terms in $g(q_0)$ and $g(-q_0)$, we obtain two coupled equations

$$H_0 g(q_0) + H_-(q_1, -q_0)g(-q_0) = 0$$
$$H_+(q_1, q_0)g(q_0) + H_0 g(-q_0) = 0$$

(note $H_-(q_1, -q_0) = H_+(q_1, q_0)$).

Setting the determinant of the coefficients equal to zero, writing $\omega = Vq_s - i\Gamma_q$, and solving for Γ_q, we obtain

$$\Gamma_q = \Gamma_{q_0} \pm \tfrac{1}{2}G_q \tag{17}$$

where

$$G_q = \frac{1}{2\rho_0}\Big[(\nu_5 - \nu_4 + 2\nu_3 - \nu_2)(q_s^2 + 2q_0^2)\sin^2\theta + (\nu_5 - \nu_4 + \nu_2)2q_0^2\sin^2\theta + (\nu_1 + \nu_2 - 2\nu_3)\sin^4\theta\, q_s^2\Big]. \tag{18}$$

Let us collect the principal results of the above calculations. We have derived three expressions which are valid in three regemes

1) For $q_3 \gg q_0$ or $q_3 \ll q_0$

$$\Gamma_q = (\Gamma_q)_0.$$

2) For q_3 slightly greater than q_0

$$\Gamma_q = (\Gamma_q)_0 + \tfrac{1}{2}G_q.$$

3) For q_3 slightly less than q_0

$$\Gamma_q = (\Gamma_q)_0 - \tfrac{1}{2}G_q.$$

In particular, at $q_3 = q_s\cos\theta = q_0$ there exists a "band gap" in the attenuation given by

$$G_q = \frac{q_s^2}{2\rho_0}\Big[\{5(\nu_5 - \nu_4) + 6\nu_3 + \nu_2\}\sin^2\theta - \{4(\nu_5 - \nu_4) + 6\nu_3 - \nu_1 - \nu_2\}\sin^4\theta\Big] \tag{19}$$

The anomaly in the vicinity of the band gap has been called the Brillouin zone effect by Parsons and Hayes.

Twisted nematic model

Lubensky has shown that the sound velocity in cholesterics is anisotropic.[2] The difference in the elastic constants corresponding to propagating sound

parallel and perpendicular to the pitch axis is given, in our notation, by

$$C_{33} - C_{11} = K_2' \left[\frac{q_0^2}{\rho} - 2q_0 \left(\frac{2q_0}{\partial \rho} \right)_{hs} \right]$$

where K_2' is the bend elastic constant for the director, $q_0 = 2\pi/\lambda_0$ where λ_0 is the pitch, and h is a field conjugate to a change in λ_0. In this expression the first term is always positive. The second term is positive or negative depending on the sign of $[\partial q_0/\partial \rho]_{hs}$ and if we assume that it is very small compared to the first term we arrive at an anisotropy in the velocity of the order of 0.1 cm/sec.[14] Previous data showed that the measured anisotropy is orders of magnitude higher and has the opposite sign. Because the measurements were made at finite frequencies, the sign and magnitude of the anisotropy could be due to dispersive effects. In order to analyze the data quantitatively we will use a "twisted nematic" model.

When a sound wave propagates along the pitch axis, i.e., $\hat{n} \perp \hat{q}_s$, we have a situation which correspond to the minimum velocity configuration for a nematic. However, when the sound wave propagates perpendicular to the pitch axis, the angle between $\hat{n}$ and $\hat{q}$ varies from 0° to 180° as the sound travels through one pitch-length. Thus the elastic constants C_{11} and C_{33} are both sampled and a larger velocity is expected.

We assume that the nematic elastic constant matrix for $\hat{n}$ parallel to the 3-axis, is of the form

$$C_{ij} = \begin{bmatrix} C_{11} & C_{11} & C_{13} & 0 \\ C_{11} & C_{11} & C_{13} & \\ C_{13} & C_{13} & C_{33} & \\ 0 & & & 0 \end{bmatrix}$$

at a particular frequency ω. If we now twist (rotate) the director about the 2-axis by an angle Φ,[14] and average over Φ, we obtain a new elastic stiffness matrix given by

$$\bar{C}_{kl} = \frac{1}{8} \begin{bmatrix} 3C_{11} + 2C_{13} + 3C_{33} & 4(C_{11} + C_{13}) & C_{11} + 6C_{13} + C_{33} \\ 4(C_{11} + C_{13}) & 8C_{11} & 4(C_{11} + C_{13}) \\ C_{11} + 6C_{13} + C_{33} & 4(C_{11} + C_{13}) & 3C_{11} + 2C_{13} + 3C_{33} \end{bmatrix}$$

Therefore the elastic constants for our twisted nematic model of a cholesteric are given by

$$\begin{aligned} \bar{C}_{11} &= \tfrac{1}{8}(3C_{11} + 2C_{13} + 3C_{33}) \\ \bar{C}_{33} &= C_{11} \\ \bar{C}_{13} &= \tfrac{1}{2}(C_{11} + C_{13}) \end{aligned} \tag{20}$$

Substituting this in our general expression for the velocity, we obtain the following expression for anistropy for the case $C_{13}^2 = C_{11}C_{33}$

$$V^2(\theta) = \bar{C}_{11} + (\bar{C}_{33} - \bar{C}_{11})\cos^2\theta \tag{21}$$

Here the velocity anisotropy has the right sign and, compared to typical values for nematics, the right order of magnitude.

Forster, *et al.*,[4] calculated an expression for the attenuation anisotropy in nematics. The viscosity matrix is of the form

$$v_{ij} = \begin{bmatrix} \nu_4 + \nu_2 & \nu_4 - \nu_2 & \nu_5 & & \\ \nu_4 - \nu_2 & \nu_4 + \nu_2 & \nu_5 & & 0 \\ \nu_5 & \nu_5 & 2(\nu_5 + \nu_1) - \nu_4 + \nu_2 & & \\ & 0 & & \nu_3 & \\ & & & & \nu_3 \\ & & & & & \nu_2 \end{bmatrix}. \tag{22}$$

Identifying $D_{11} = \nu_4 + \nu_2$, $D_{33} = 2(\nu_5 + \nu_1) - (\nu_4 - \nu_2)$, $D_{13} = \nu_5$, and $D_{44} = \nu_3$ one gets their expression for the attenuation, neglecting the thermal conductivities.

Proceeding in the same way as before we obtain an averaged $\bar{D}_{ij}$ matrix of the form

$$\begin{aligned} \bar{D}_{11} &= \tfrac{1}{8}[3D_{11} + 2D_{13} + 3D_{33}] = \nu_5 + \tfrac{3}{4}(\nu_1 + \nu_2) \\ \bar{D}_{33} &= D_{11} = (\nu_4 + \nu_2) \\ \bar{D}_{13} &= \tfrac{1}{2}(D_{12} + D_{13}) = \tfrac{1}{2}(\nu_5 + \nu_4 - \nu_2) \\ \bar{D}_{44} &= \tfrac{1}{2}(D_{44} + D_{66}) = \tfrac{1}{2}(\nu_3 + \nu_2) \end{aligned} \tag{23}$$

Substituting in the expression for α we obtain

$$\alpha(\theta) = \frac{\omega^2}{2\rho V^3}\left\{(\nu_4 + \nu_2) + (\nu_5 - \nu_4 + 2\nu_3 - \nu_2)\sin^2\theta + [\tfrac{3}{4}(\nu_1 + \nu_2) - 2\nu_3]\sin^4\theta\right\} \tag{24}$$

Compared with Eq. (14) we find that there is an additional term $\frac{1}{2}\nu_3 \sin^4\theta$. However, both expressions predict the same behavior for the anisotropy and the magnitude of the anisotropy differs very little because of the smallness of

v_3. The twisted nematic model calculation, however, fails to give the expression for the band-gap because the model is only valid in the hydrodynamic limit, i.e., $q_s \ll q_0$. We will be using the Eq. (14) to calculate the combinations of v_i's from our data.

Section III. Experimental data and analysis

The material chosen for study is a mixture of cholesteryl chloride and cholesteryl myristate (1.75:1 by weight). It has a negative magnetic anisotropy and, as explained in the introduction, can be oriented macroscopically. In addition CC-CM has a very interesting property: the two constituents have opposite helicity and, near 42°C (hereafter referred to as T_N), they compensate each other completely giving rise to a cholesteric with infinite pitch, i.e., a nematic. Below T_N however the pitch changes sign and becomes finite again. Therefore this material is particularly suited to study the anisotropic attenuation for the different regimes of q_3/q_0, as specified by Eqs. (14) and (18).

In this section, we describe anisotropic sound propagation in the region where the Brillouin Zone effect is unimportant. Two sonic cells—one with a fixed path and the other with a variable path—were used at different stages of the experiment. Both cells have been described elsewhere.[14] With the variable-path cell we could determine the absolute velocity and attenuation within $\pm 0.5\%$ and $\pm 1\%$ respectively; relative measurements gave an accuracy of $\pm 0.1\%$ and $\pm 0.5\%$ respectively. The measurements were carried out using the phase matching technique. The temperature of the cells was automatically controlled to ± 0.01°C. All measurements were done at a frequency of 4 MHz.

The cells were placed between the pole-pieces of an Arthur D. Little (Bitter type) electromagnet, the strength of which could be varied continuously up to ~ 28 kG.

Figure 1 shows a temperature sweep of the velocity and attenuation for a magnetic field, H, of 28 kG and an angle, θ, between $\mathbf{H}$ and q_s of 0°. Note the sharp rise of attenuation at 68°C—the temperature of isotropic-cholesteric transition. This trace does not show the fine-structure of the attenuation near T_N; this feature will be discussed later.

Previous experiments on this material showed a history-dependent velocity anisotropy when the magnet was rotated while the material was in the cholesteric phase. A small history-dependence at orientations near $\theta = 0°$. and $\theta = 90°$ suggested the possible existence of boundary or texture effects which presumably prevent complete reorientation. Also no attenuation anisotropy was observed within the accuracy of those measurements. All these effects suggested that the magnetic field strength of 12 kG was insufficient to overcome the boundary anchoring and rotation induced texture effects.

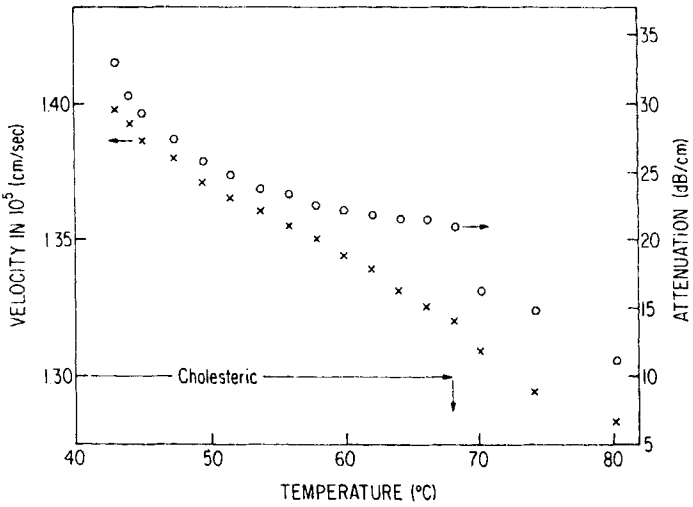

FIGURE 1 Temperature dependence of velocity and attenuation with the field parallel to the sound propagation direction.

Figure 2 shows the velocity anisotropy when the magnet was rotated in the cholesteric phase. The hysteresis, though smaller, is still present. The magnitude of the anisotropy is substantially greater indicating a larger degree of realignment.

Figure 3 shows the attenuation anisotropy which was observed for the first time; this effect also had a finite hysteresis. Each point was obtained after waiting for a time sufficiently long that a metastable equilibrium was established. Figure 4 shows the variation of velocity with time following a field rotation in the cholesteric phase. The slow response of the molecules can be characterized by a relaxation time τ. The experimental data could be very well represented by a growth function of the form $(1 - e^{-t/\tau})$. Figure 5 shows the variation of τ with the field strength H. The shape of the curve is consistent with a field dependent relaxation time of the form

$$\frac{1}{\tau(H)} = \frac{aH^2}{1 + bH^2} \tag{25}$$

For a temperature of 57.9°C we find

$$a = 0.4 \times 10^{-3}\ \text{min}^{-1}\ \text{kG}^{-2}$$
$$b = 0.4 \times 10^{-5}\ \text{kG}^{-2}$$

Here $\tau(\mathscr{H})$ is measured in the bulk; for thin films, it can be quite different. Using this curve we could estimate how much time one should allow for the

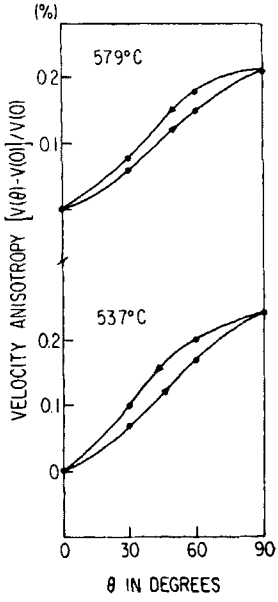

FIGURE 2 Velocity anisotropy produced by rotating the field in the cholesteric phase. The arrows indicate the way the field was rotated.

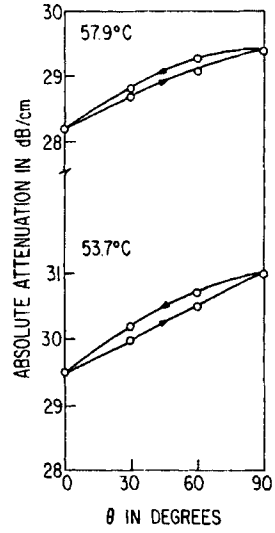

FIGURE 3 Attenuation anisotropy produced by rotating the field in the cholesteric phase. The arrows indicate the way the field was rotated.

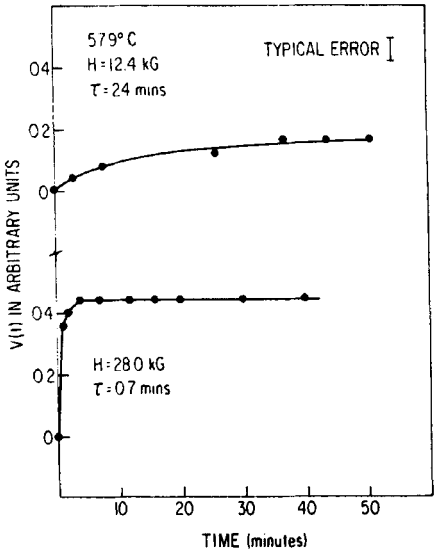

FIGURE 4 Velocity change after the field was rotated in the cholesteric phase.

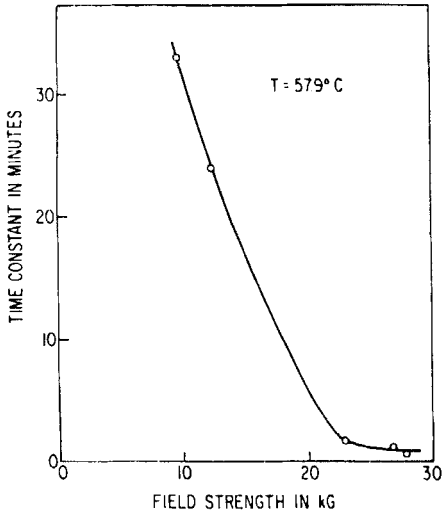

FIGURE 5 Field-dependence of the relaxation time τ.

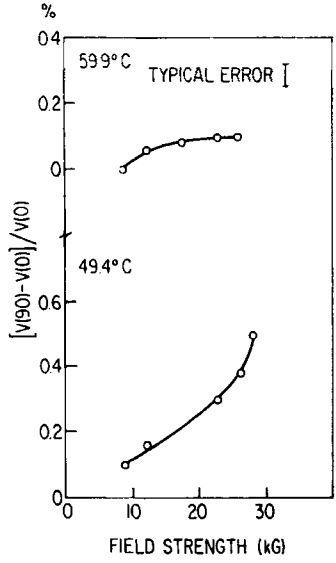

FIGURE 6 Field-dependence of the magnitude of the velocity anisotropy produced by rotating the field in the cholesteric phase.

material to come to equilibrium. However, some degree of hysteresis still remained after waiting what appeared to be a reasonable time. Clearly texture and boundary effects could not be completely overcome with the available field.

Figure 6 shows the field dependence of the magnitude of the anisotropy $|V(90°) - V(0°)|$, at two different temperatures. At the higher temperature and with the maximum available field strength, a tendency toward saturation is observed. But at the lower temperature saturation is not seen. This also indicates the inadequacy of the field-strength to obtain nearly complete reorientation.

The largest anisotropies, implying the highest degree of alignment, were obtained using the field-cooling technique, i.e., the sample was heated into the isotropic phase followed by a slow cooling into the cholesteric phase at a desired angle. This was done for each angle and the resulting anisotropy in velocity and attenuation are shown in Figure 7. The observed increase in magnitude of the anisotropy points towards a higher degree of realignment. With the field cooling technique saturation was observed above 15 kG. Taken together these observations imply a nearly complete alignment.

Figure 8 shows the temperature variation of $\bar{C}_{11}$ and $\bar{C}_{11} - \bar{C}_{33}$ calculated from Eq. (21). From the twisted nematic model they are related to the corresponding nematic stiffness coefficients. The anisotropy is fairly large

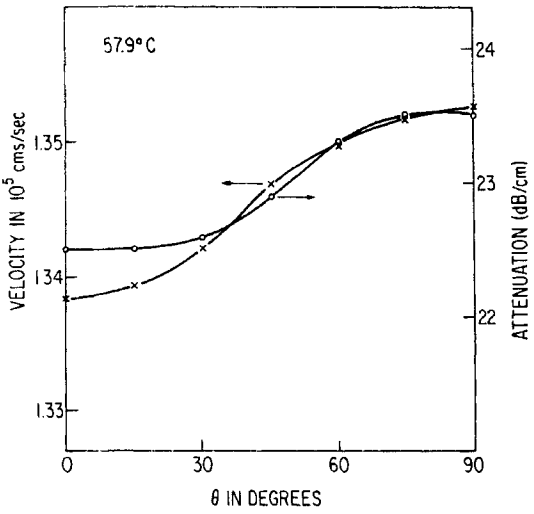

FIGURE 7 Velocity and attenuation anisotropy in the cholesteric phase. Produced by cooling the material from the isotropic phase in a particular field-direction.

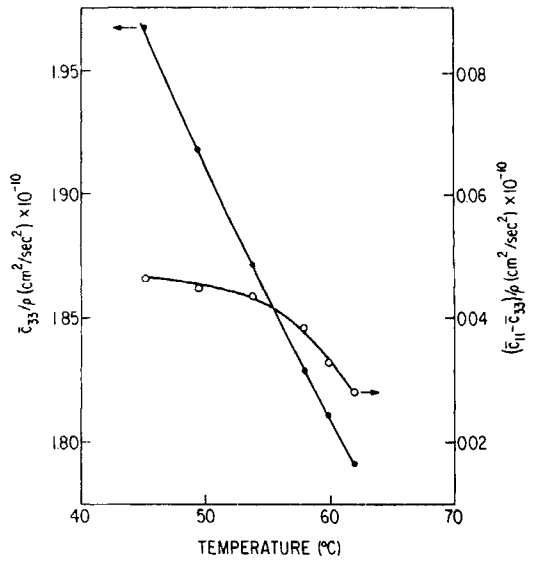

FIGURE 8 Temperature dependence of $\bar{C}_{11}$ and $\bar{C}_{11}-\bar{C}_{33}$ in the cholesteric phase.

compared to Lubensky's prediction, and of the opposite sign. However, if we assume that dispersion, similar to that observed in nematics, is present in the cholesteric, then the twisted nematic model appears to explain the sign and magnitude of the anisotropy reasonably well. The zero-frequency limit, however, could not be ascertained without measurements performed at other frequencies.

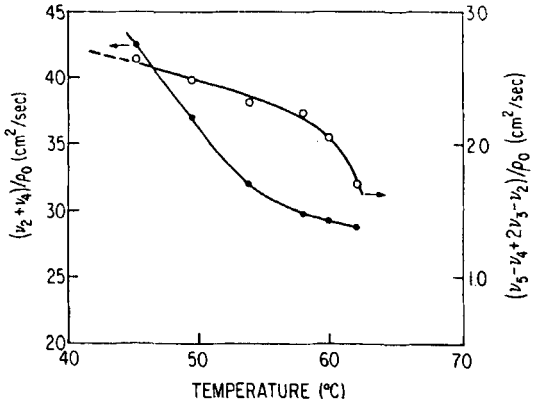

FIGURE 9 Temperature dependence of two combinations of the viscosity coefficients in the cholesteric phase.

Figure 9 shows the temperature variation of two combinations of the viscosity coefficients. Within our resolution no intermediate maximum or minimum was seen, indicating that the $\sin^2\theta\cos^2\theta$ term in the expression for the attenuation is rather small. With this assumption, both the expressions derived for attenuation from the twisted nematic model and the hydrodynamic equations relevant to the cholesterics give us the same result

$$\alpha(\theta) = \frac{\omega^2}{2\rho_0 V^3}\left[(\nu_2 + \nu_4) + (\nu_5 - \nu_4 + 2\nu_3 - \nu_2)\sin^2\theta\right]. \tag{26}$$

Observe that from Kemp and Letcher's data, the $\sin^2\theta$ term would become positive for the values of ν_i they obtained. This would produce an anisotropy of the observed sign. Figure 9 shows the temperature dependence of $(\nu_2+\nu_4)/\rho_0$ and $(\nu_5-\nu_4+2\nu_3-\nu_2)/\rho_0$. These values were obtained by least-square fitting the data using Eq. (26). Here also we have assumed that the contribution from the thermal conductivities is very small compared to the viscosities.

Section IV. Brillouin-zone effect

In this section we give a more detailed report of the acoustic Brillouin-zone effect which was reported earlier.[12] The theory has been discussed in Section II. It has been noted that an accurate measurement of attenuation is necessary in order to see this effect. A block diagram of the electronics is shown in Figure 10. The c.w. output of the high-frequency signal generator was fed to two co-axial crystal switches which were alternately activated by a square-wave generator. The output of the switches were applied to the sonic-cell and a precision attenuator (which was adjustable to 0.1dB steps). The outputs of the sonic cell and the attenuator were combined at the receiver input; the receiver output was then applied to a lock-in amplifier which was also driven by the squarewave generator. When the amplitude of the two signals (one coming from the cell and the other from the attenuator) were equal, no a.c. component arrived at the lock-in output. Using the amplitude of the lock-in to interpolate between the 0.1dB steps of the attenuation, a resolution of better than 0.005dB was routinely achieved. The period of oscillation was $\sim 10^4 \mu$ sec which was much longer than the transit time through the sonic cell ($\sim 1\mu$ sec) and thus steady-state conditions were achieved. The round-trip attenuation in the cell was greater than 12dB in the temperature range of interest; thus the presence of standing waves produced a negligible distortion of the results. Furthermore, the electromagnetic feedthrough between the transmitter and the receiver was negligible. A second experimental arrangement was also employed. Here the signal generator was frequency modulated and any amplitude modulation of the signal traversing the sonic cell (resulting from a frequency dependence of the attenuation, transducer characteristics,

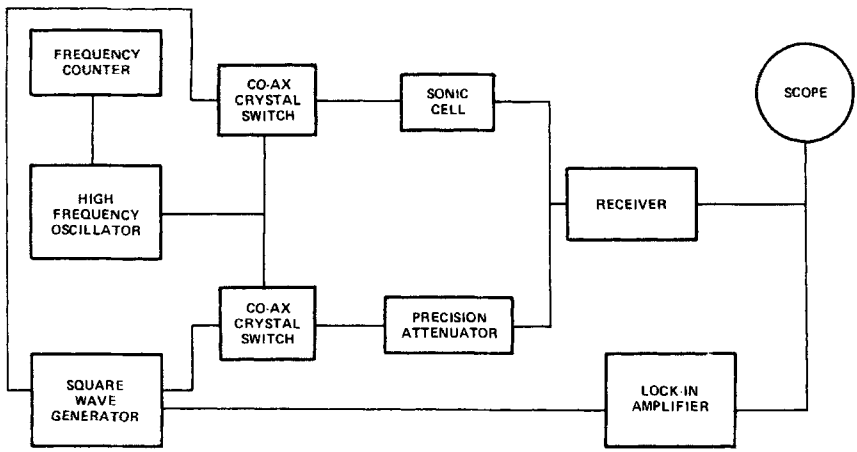

FIGURE 10 Block diagram of the electronics used for Brillouin zone effect measurement.

etc.) was detected by a lock-in amplifier (the r.f. switches were not employed in this configuration). We expected strong amplitude modulation only in the vicinity of the Bragg condition.

All measurements were done at 4 MHz. The acoustic path-length was 2 mm and the temperature stability was ± 0.01°C. From the measurements reported in Section III, the velocity of sound at 42°C was found to be 1.402×10^5 cm/sec which results in a $q_s = 179.4\,\text{cm}^{-1}$.

Figure 11 shows a plot of attenuation versus temperature for an angle of 30° between the magnetic field **H** the strength of which is 28 KGauss, and the sound propagation direction, $\mathbf{q}_s$. Note that a gap appears at 42.8°C and a sharp change in slope appears at 41.6°C. This can be interpreted in the following way: light scattering measurements[14] showed that the pitch is a strong function of temperature, being infinite near 42°C. The two points corresponding to 42.8°C and 41.6°C represent identical pitches but opposite helicity. However, since the Brillouin-zone boundary is approached from opposite directions, the direction in which the attenuation changes should be opposite, i.e., the lower temperature gap should mark a sharp decrease in attenuation. It was noted, however, that in that temperature range the background attenuation rises very rapidly. The flat part of the attenuation curve

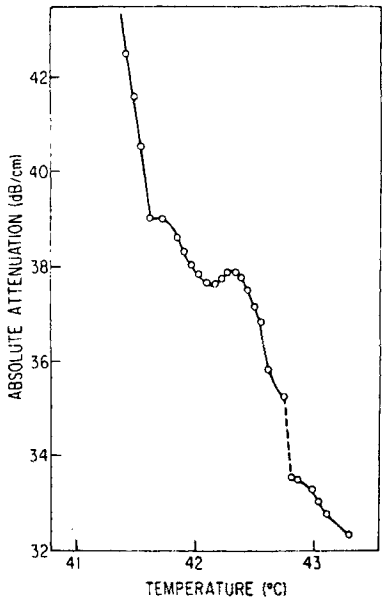

FIGURE 11 Temperature dependence of the attenuation. The angle between $\mathbf{q}_s$ and $\mathbf{q}_0$ is 30°. A gap appears at 42.8°C and a sharp discontinuity occurs at 41.6°C. Note an anomaly occuring at the nematic point.

just preceeding the drastic change of slope presumably results from the combined effects of a small temperature inhomogeneity together with the competing effects of the zone-effect and the back-ground attenuation. Note that ananomaly in the attenuation occurs around the point where the pitch is infinite, i.e., where the material is nematic. Since no phase transition is expected at that point,[17,18] this anomaly must arise from a different mechanism.

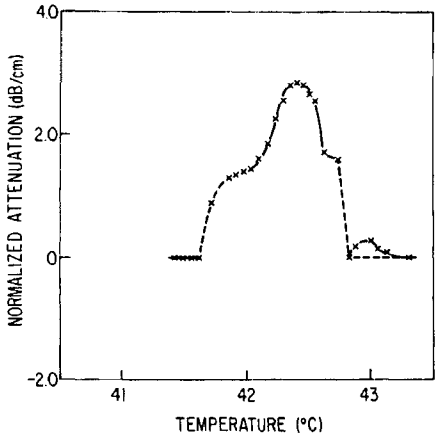

FIGURE 12 The same as Figure 11 with a suitable background subtracted. Gaps appear at 42.8°C and 41.6°C.

Figure 12 shows the same temperature sweep as Figure 11 with the estimated background subtracted. Two gaps now appear in the attenuation. Figure 13 shows plots of attenuation versus temperature for angles 45°, 60° and 75°. It would be interesting to investigate the nature of the anisotropy in this region. The solutions to the equations, however, are quite complicated for the intermediate range of values of q_0/q_s which are appropriate here. In addition, at T_N the director can be anywhere in the plane perpendicular to the field for an infinite sample; in a finite sample, the orientation is presumably determined by the boundary conditions which are quite complicated in our experimental geometry.

As was discussed in Section III, for each angle the material was field-cooled from the isotropic phase. For each temperature sweep a total time of approximately 10 hours was required. Data collected at a faster rate were found to be less reproducible, presumably because of a lack of a uniform macroscopic orientation in the sample.

For each angle, q_3, the component of $\mathbf{q}_s$ along $\mathbf{q}_0$ is different and therefore the Bragg-like condition is met at a different temperature because of the

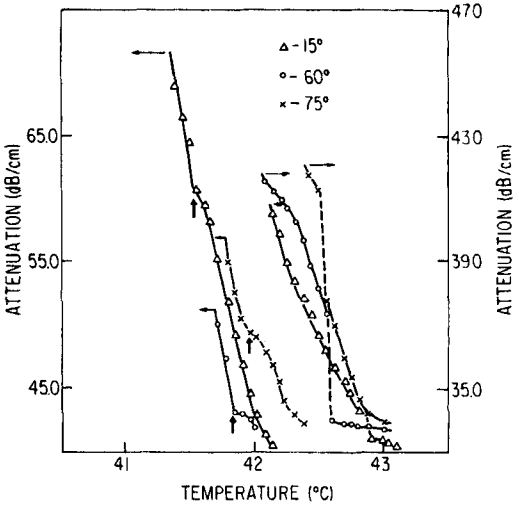

FIGURE 13 Absolute attenuation versus temperature. The angle between $\mathbf{q}_s$ and $\mathbf{q}_0$ are 15° (triangles), 60° (circles), and 75° (crosses).

strong temperature dependence of the pitch. The two gaps were assumed to be symmetrically spaced about T_N which was calculated to be 42.2°C. The temperature dependence of the pitch calculated from the Bragg condition is shown in Figure 14. The data were fitted to the relation

$$P = a/(T - T_N) \tag{26}$$

which yields the value 130μ°C for a which is somewhat higher than that obtained in the light-scattering experiment. This could be attributed to the fact that small difference in concentration may change the rate of compensation between the competing constituents of the material. This is also evidenced in the fact that T_N is also slightly different from the quoted value of 42°C. It is also possible that the temperature dependence is more complicated than that given by Eq. (26).

For different angles the magnitudes of the gaps were measured. The angular dependence of the higher temperature band-gap is shown in Figure 15. This was fitted to Eq. (18) of Section II from which we derive the following values:

$$\frac{1}{\rho_0}(5\nu_5 - 5\nu_4 + 6\nu_3 + \nu_2) = 9.3 \text{ cm}^2/\text{sec}$$

$$\frac{1}{\rho_0}(\nu_5 - \nu_4 + \nu_1 + 2\nu_2) = 6.3 \text{ cm}^2/\text{sec}$$

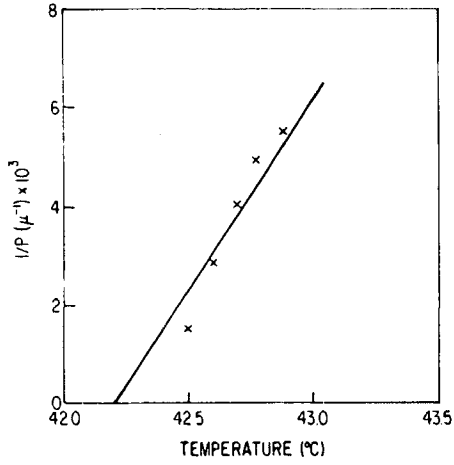

FIGURE 14 The temperature dependence of the pitch calculated from the Bragg condition. The inverse pitch is plotted against temperature and the straight line is a fit using Eq. (22) with $T_N = 42.2°C$.

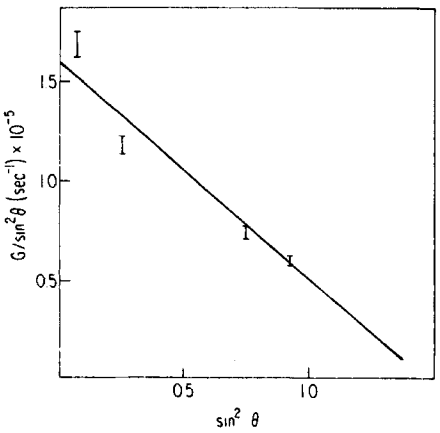

FIGURE 15 Angular dependence of the magnitude of the band-gap. The straight line is a fit using Eq. (15).

Experiments at higher frequencies were not performed due to the rapid increase in the attenuation with frequency. However, Figure 16 shows the results of the frequency modulation experiment at $\theta = 45°$. A very large peak in $\partial\Gamma/\partial f_s$ is seen as the temperature is swept through the value of $q_0(T)$ satisfying the Bragg-condition. This would appear to eliminate any other interpretation (e.g., involving a geometrical or size effect) of the data.

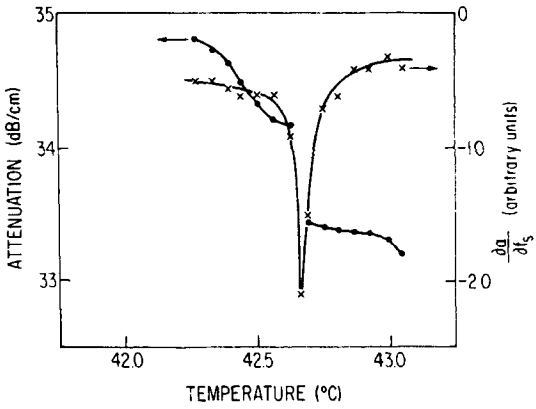

FIGURE 16 The absolute attenuation and its frequency-derivative plotted against temperature. The angle between $\mathbf{q}_s$ and $\mathbf{q}_0$ is 45°.

Acknowledgment

We wish to thank Dr. C. W. Woo and Dr. K. Miyano for useful discussions.

References

1. J. L. Ericksen, *Arch. Rational Mech. Anal.* **4**, 231 (1960). F. M. Leslie, *Quart. J. Mech. Appl. Math.* **19**, 357 (1966).
2. T. C. Lubensky, *Phys. Rev.* **A6**, 452 (1972).
3. P. C. Martin, P. S. Pershan, and J. Swift, *Phys. Rev. Lett.* **25**, 844 (1970).
4. D. Forster, T. C. Lubensky, P. C. Martin, P. S. Pershan, and J. Swift, *Phys. Rev. Lett.* **26**, 1016 (1971).
5. P. C. Martin, O. Parodi, and P. S. Pershan, *Phys. Rev.* **A6**, 2401 (1972).
6. W. A. Hoyer and A. W. Nolle, *J. Chem. Phys.* **24**, 803 (1956).
7. K. A. Kemp and S. V. Letcher, *Phys. Rev. Lett.* **27**, 1634 (1971).
8. M. E. Mullen, B. Luthi, and M. J. Stephen, *Phys. Rev. Lett.* **28**, 799 (1973).
9. A. E. Lord and M. M. Labes, *Phys. Rev. Lett.* **25**, 570 (1970).
10. A. E. Lord, *Phys. Rev. Lett.* **29**, 1366 (1972).
11. K. Miyano and J. B. Ketterson, *Phys. Rev. Lett.* **31**, 1047 (1973).
12. I. Muscutariu, S. Bhattacharya, and J. B. Ketterson, *Phys. Rev. Lett.* **35**, 1584 (1975).
13. E. Sackmann, S. Meiboom, and L. C. Snyder, *J. Am. Chem. Soc.* **89**, 5981 (1967).
14. K. Miyano and J. B. Ketterson, *Phys. Rev.* **A12**, 615 (1975).
15. E. Sackmann, S. Meiboom, L. C. Snyder, A. E. Meixner, and R. E. Dietz, *J. Am. Chem. Soc.* **90**, 3567 (1968).
16. J. D. Parsons and C. F. Hayes, *Solid State Commun.* **15**, 429 (1974).
17. M. J. Stephen and J. P. Straley, *Rev. Mod. Phys.* **46**, 617 (1974).
18. P. G. deGennes, Physics of Liquid Crystals (Oxford Univ. Press, Oxford, England, 1975), p. 10.
19. A. E. Lord, *Mol. Cryst. Liq. Cryst.* **18**, 313 (1972).